Journal of Magnetic Resonance 307 (2019) 106582

Contents lists available at ScienceDirect

Journal of Magnetic Resonance

journal homepage: www.elsevier.com/locate/jmr

Motion reduction for quantitative brain sodium MR imaging with a navigated flexible twisted projection imaging sequence at 9.4 T

Aiming Lu [a,*], Ian C. Atkinson [b], Keith R. Thulborn [b]

[a] Department of Radiology, Mayo Clinic, Rochester, MN 55901, United States
[b] Center for Magnetic Resonance Research, University of Illinois at Chicago, Chicago, IL 60612, United States

ARTICLE INFO

Article history:
Received 23 May 2019
Revised 16 August 2019
Accepted 20 August 2019
Available online 21 August 2019

Keywords:
Sodium imaging
Twisted projection imaging
Navigator echo
Motion correction
Eddy current correction

ABSTRACT

Quantitative measurement of the tissue sodium concentration (TSC) provides a metric for tissue cell volume fraction for monitoring tumor responses to therapy and neurodegeneration in the brain as well as applications outside the central nervous system such as the fixed charge density in cartilage. Despite the low detection sensitivity of the sodium MR signal compared to the proton signal and the requirement for a long repetition time to minimize longitudinal magnetization saturation, acquisition time has been reduced to less than 10 min for a nominal isotropic voxel size of 3.3 mm with the improved acquisition efficiency of twisted projection imaging (TPI) at 9.4 T. However, patient motion can degrade the accuracy of the quantification even within these acquisition times. Our goal has been to improve the robustness of quantitative sodium MR imaging by minimizing the impact of motion that may occur even in cooperative patients. We present a method to spatially encode a lower resolution navigator echo after encoding the free induction decay signal for the quantitative image at no time penalty. Both the imaging and navigator data are sampled with flexTPI readout trajectories. Navigator images are generated at a higher temporal resolution (~1 min) albeit at lower spatial resolution (8 mm) than the quantitative high-resolution images. The multiple volumes of navigator echo images are then aligned to extract the translational and rotational motion parameters assuming rigid-body motion. These parameters are used to align the k-space data during the acquisition of each volume of the quantitative images. Our results show significantly reduced image blurring with this method when the subject's head moved randomly by up to 7° between the navigator acquisitions.

1. Introduction

Quantitative sodium magnetic resonance imaging is a non-invasive approach for measuring regional metabolic disturbances reflected in tissue sodium concentration (TSC) caused by human brain pathology such as stroke [1,2], brain tumors [3,4] and neurodegenerative disease [5–8]. This clinically relevant information is not available from other methods [9–11]. The energy-consuming sodium-potassium ion pumps on the cell membranes tightly control the low intracellular sodium concentrations while multiple systemic endocrine systems control the high extracellular sodium concentration [12]. Disruption of the function of these pumps by pathological metabolic disturbances results in cytotoxic edema from immediate redistribution of sodium and other ions between these two tissue compartments. This redistribution does not immediately increase the TSC but as the effective sodium concentration decreases in the expanded extracellular space, more sodium ions diffuse down the concentration gradient from the vascular spaces. The sodium concentration in the vascular system is maintained via endocrine mechanisms operating through the kidneys, buffering the extracellular sodium concentration thereby increasing regional TSC at the pathological site. Thus, TSC obtained with quantitative sodium MRI provides a metric for any pathology that disrupts ion homeostasis, cell integrity or cell packing.

The intrinsic sodium MR detection sensitivity is 4–5 order lower than that of the proton and exhibits rapid bi-exponential relaxation behavior ($T2_{fast} \sim 1$–3 ms and $T2_{slow} \sim 12$–25 ms) in biological tissues. Quantitative sodium MR imaging therefore necessitates acquiring the free-induction-decay (FID) signal immediately after a short excitation RF pulse to minimize signal loss due to transverse relaxation while using long repetition times (TRs) to minimize the saturation of longitudinal magnetization. Efficient sequences such as twisted projection imaging (TPI) [13], density adapted 3D radial acquisition [14], flexible TPI (flexTPI) [15] and 3D cones [16] have

* Corresponding author at: Mayo Clinic, OPUS Building, 200 1St Street SW, Rochester, MN 55905, United States.
E-mail address: lu.aiming@mayo.edu (A. Lu).

https://doi.org/10.1016/j.jmr.2019.106582
1090-7807/

been proposed to fully sample the FID signal in k-space with a smaller number of repetition times. Reasonable signal-to-noise ratio and spatial resolution can be achieved in acquisition times of about 10 min for quantitative sodium imaging but additional time is often required for B_0 and B_1 field corrections [15]. Head motion can therefore present a significant source of quantification error, in even a cooperative patient over such a relatively long time.

Several motion compensation methods have been proposed for proton MR imaging. Motion can be detected from data obtained from the MR scanner or from other external devices such as cameras [17–20]. External tracking systems allow for rapid motion detection without interrupting MR imaging but require dedicated devices that are not widely available and may complicate imaging setup and/or compromise patient comfort (e.g., placement of reflective objects). Direct motion detection with MR signals is therefore desirable if the time impact of acquiring the motion correction data (i.e., MR images, navigators) is minimized.

We propose a navigator-based retrospective motion correction to compensate for motion during quantitative sodium imaging without any increase in acquisition time. The flexTPI sequence was modified to form a gradient echo after acquiring the FID signal with the flexTPI readout. The echo was then sampled using a different set of flexTPI trajectories to acquire the navigator echo images at lower spatial but higher temporal resolution than that for the quantitative images generated from the FID signal. Assuming rigid-body motion, the extracted translational and rotational motion parameters between the navigator images were then used to align the quantitative sodium imaging data in k-space. As the radial-acquisition based flexTPI sequence is sensitive to eddy currents induced by the time-varying readout gradient, the k-space trajectories were measured to obtain both the spatial independent term (B_0 eddy currents) and the linearly spatial dependent term (linear eddy currents) simultaneously on a phantom [21,22], which were then used to compensate for eddy currents during image reconstruction.

2. Materials and methods

2.1. Modified flexTPI sequence with navigator acquisition (navTPI)

The navTPI sequence proposed to acquire an additional navigator echo for motion correction is illustrated in Fig. 1. Following a short hard excitation RF pulse, the FID signal was immediately sampled in k-space using flexTPI readout trajectories designed for quantitative sodium imaging [15]. The remaining transverse magnetization was then refocused to form the navigator echo signal, and sampled with another set of flexTPI readout trajectories at a lower spatial resolution. Multiple frames of navigator images were acquired during the acquisition of one image set used for quantification without increasing the total acquisition time.

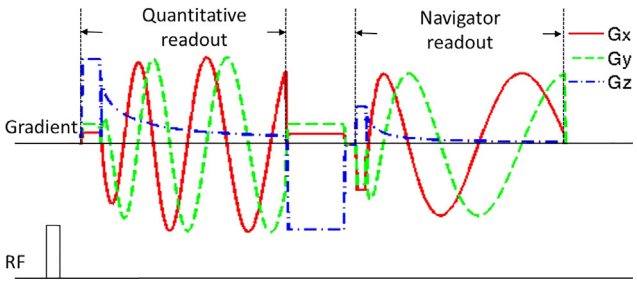

Fig. 1. Pulse sequence diagram of the navTPI sequence. Following the radio frequency (RF) pulse, the quantitative readout with flexTPI gradient trajectories (Gx solid line, Gy dashed line, Gz dash-dot line) is performed over ~9.8 ms, followed by gradient reversal to generate a gradient echo that is then sampled with different flexTPI gradient waveforms producing the navigator readout over 7.7 ms.

2.2. Eddy current characterization

Radial acquisition based k-space sampling strategies such as flexTPI are sensitive to gradient timing errors and eddy currents induced by the varying readout gradient. A previously proposed method [23,24] was adopted to measure the timing errors on the three physical axes, which were then used to align the gradient waveforms with the analog-to-digital converter (ADC). To compensate for eddy currents induced by the time-varying readout gradient, the method proposed in [21] for measuring the k-space trajectories generated by a certain gradient waveform was extended to characterize both B_0 and linear eddy currents, as has been done in [22]. On each physical axis, the FID signal following a hard RF pulse was first phase-encoded and then sampled in the presence of the gradient waveform under investigation on that axis. This was repeated with n phase encoding steps and the waveform at m gradient amplitudes for a total of $n \times m$ acquisitions. The acquired signal $s(t, j)$ for the jth phase encoding can be written as:

$$s(t,j) = \int m(r) e^{i\left\{\left(\hat{k}(t)r + \hat{\phi}_{B0}(t)\right)g + j\Delta k_{pe} r + \phi(r,t)\right\}} dr \quad (1)$$

where $m(r)$ is the magnetization, r is the spatial location in the phase encoding direction, g is the gradient amplitude, $\hat{k}(t) = \frac{1}{g}\int_0^t (G(\tau) + e_l(\tau))d\tau$ is the normalized k-space trajectory including the linear eddy current term $e_l(\tau)$ induced by the gradient waveform $G(\tau)$, $\hat{\phi}_{B0}(t)$ is the phase accumulated by B0 eddy currents, also normalized by g, Δk_{pe} is the phase encoding step size, $\phi(r,t)$ is the phase from all other sources. The number of phase encodings required is: $N \geq k_{\max} FOV_{pe}$, where $k_{\max}$ is the maximum k-space radius accumulated by the gradient under investigation and FOV_{pe} is the FOV used in the phase encoding direction. The signal after the 1D Fourier transform along the phase encoding direction is:

$$s(r,t) = m(r) e^{\left(\hat{k}(t)r + \hat{\phi}_{B0}(t)\right)g + \phi(r,t)} \quad (2)$$

Similar to [22], linear least square fitting was first performed to extract $\hat{k}(t)$ and $\hat{\phi}_{B0}(t)$, which were then used during image reconstruction.

The navTPI sequence collects k-space data on a stack of symmetric concentric cones. In one hemisphere, the three components of a representative trajectory on the physical axes were measured separately on each cone. Other trajectories were calculated by rotating the measured trajectories on the corresponding cones. The trajectories in the other hemisphere were calculated based on symmetry. The gradient waveforms on Z-axis in the navTPI sequence only differ in scale and therefore only needed to be measured once on a representative cone, which reduced the total acquisition time for collecting eddy current correction data by nearly 1/3. The same eddy current characterization and correction was performed separately on both the quantitative readout gradient waveforms and the navigator readout gradient waveforms.

2.3. Simulation of impact of motion on quantification

A numerical phantom consisting of a central region of cerebrospinal fluid (CSF; $2.6 \times 4.9 \times 2.6$ cm^3, 145 mM, T_2 = 55 ms) surrounded by tissue ($10 \times 10 \times 10$ cm^3, 36 mM, biexponential T_2 of 60% 2.5 ms and 40% 14 ms) was used to investigate the effect of intra-acquisitional motion on quantification. The k-space data corresponding to a 10-min flexTPI acquisition were simulated with random, smoothly varying 3D translations (peak-to-peak

0.05–2.5 mm) and 3D rotations (peak-to-peak 0.05–2.5°) during the acquisition using customized software in Matlab (Mathworks, Natick, MA). Images reconstructed from the data were then converted to TSC bioscales, and the percent signal differences from the motion-free acquisition were computed across the phantom.

2.4. MR imaging

All imaging was performed using customized single-tuned quadrature transmit/receive ^{23}Na volume RF coils on a 9.4 T scanner designed for human head imaging [15,24]. Static field (B_0) homogeneity was manually optimized using room temperature shim coils (up to 3rd order). As this scanner is above the FDA guideline for static magnetic field exposure for humans, this work was performed under an investigational device exemption (IDE) from the Food and Drug Administration (FDA) as part of human safety testing, with approval from the Institutional Review Board (IRB) and with informed consent from volunteers. No adverse effects from the ultra-high field strength exposure [25–29] have been documented for humans.

2.5. Eddy current data collection

Eddy current correction data were collected on a spherical phantom of 16 cm inner diameter filled with 40 mM NaCl solution. For each gradient waveform measurement, i.e., one component of a k-space trajectory, 160 phase steps were used to encode a FOV of 20 cm to achieve a slice thickness of 1.25 mm. The TR used was 100 ms. The k-space trajectories for both the imaging gradients and the navigator gradients were measured.

2.6. Sodium MR imaging

The navTPI sequence was used for imaging on both healthy volunteers and the calibration phantom. Acquisition parameters used for quantitative imaging were: FOV/resolution/radial fraction/gradient strength/readout duration/number of projections/TE = 20 cm/3.3 mm/0.32/5 mT m^{-1}/9.8 ms/3657/0.26 ms (TE = 1.26 ms for B0 mapping data acquisition). Acquisition parameters for the navigator acquisition were: FOV/resolution/radial fraction/-gradient strength/readout duration/number of projections = 20 cm/8 mm/0.22/5 mT m^{-1}/7.7 ms/438. The slightly shorter readout duration for the navigator acquisition was intended to avoid significant image distortion due to the increased sensitivity to B0 inhomogeneity given its lower spatial resolution. A TR of 160 ms was used to avoid longitudinal magnetization saturation, resulting in an acquisition time of 70 s for each navigator frame. Unless otherwise mentioned, the transmit power level was manually adjusted to achieve a global $\pi/2$ excitation pulse and the scan time for each quantitative image acquisition was 9 min and 45 s.

To demonstrate the impact of motion and the proposed motion correction method, two sets of quantitative ^{23}Na image acquisitions were performed on a healthy volunteer. Each set of acquisitions contained three separate scans, one each for quantification, B_0 correction and B_1 correction (flip angle = $\pi/4$), respectively. Dataset **A** was collected with the subject remaining stationary, while dataset **B** was collected with the subject deliberately coughing and/or briefly adjusting head location in a random fashion at the beginning of the 2nd to 8th navigator frames in each acquisition.

One set of quantitative acquisitions was repeated on the calibration phantom designed to have a similar electrical loading as an average human head for this RF coil. The calibration phantom, used for converting the sodium signal to sodium concentration, contained three compartments with known sodium concentrations (30, 70, 110 mM sodium chloride in 3% agar) surrounded by a sphere (16 cm diameter) filled with potassium chloride (60 mM).

2.7. Image registration and motion correction

The three-dimensional low-resolution navigator data were aligned using the automatic image registration (AIR) software [30,31] assuming that only rigid-body motion was involved. The derived translational and rotational motion parameters were then used to compensate the k-space data acquired in the corresponding segments for motion on a point-wise basis during imaging reconstruction [32].

Image reconstruction was based on gridding with a Kaiser-Bessel kernel and 2× oversampling followed by inverse Fourier transform [15]. Motion parameters were obtained by aligning the navigator images to the first navigator images acquired during the acquisition of dataset **A**. These motion parameters were then used to correct for motion in the segments of quantitative imaging data collected during the corresponding navigator image acquisition. A frequency segmented conjugate phase reconstruction was used to correct for image distortion due to B_0 inhomogeneity [33]. TSC maps were obtained using the calibration curve derived from the phantom after compensating for B_1 inhomogeneity in both the human and phantom images.

3. Results

3.1. Eddy current correction

Representative k-space trajectories of the quantitative readout gradient on one cone and the corresponding eddy currents measured on all three axes are shown in Fig. 2. The linear eddy currents resulted in a k-space deviation of up to ~20% of the k-space interval over the readout time (Fig. 2b). While the B_0 eddy currents on the x- and y-axes are relatively small (the accumulated phases by the B_0 eddy currents during the readout were <0.02 rad or 1°), the effect of B_0 eddy currents on z-axis is significantly higher with a maximal accumulated phase of ~0.37 rad or 21° during the readout) (Fig. 2c).

The effect of eddy current correction on image quality can be appreciated in Fig. 3. The images reconstructed from the dataset **A** (no motion) without eddy current correction (Fig. 3**A**) show appreciably lower signal intensity towards the center of the images and there is a darker rim around the bright lateral ventricles as indicated by the arrows. The corresponding images reconstructed from the same data with eddy current correction show more consistent signal intensity across the field of view and minimal dark rim around the lateral ventricles (arrows).

3.2. Simulation of impact of motion on quantification

Fig. 4 shows the grayscale images of the simulation phantom and the % error of the cross-sections through the phantom for different simulated translational and rotational motions. Although the grayscale images are visually identical, quantification errors increase significantly as the amount of motion increases, as is evident in the difference images. The errors are not only most pronounced near high-contrast borders, but also extend across homogenous regions of the phantom. Acceptable errors of less than 5% of the TSC bioscale can only be obtained for the smallest movements (<0.25 mm maximum translation and <0.25° maximum rotation), which are considerably less than the voxel resolution.

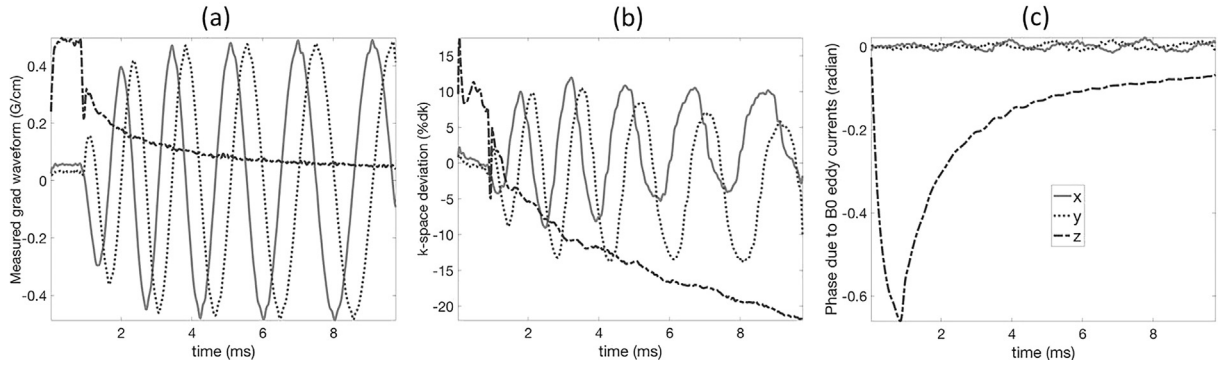

Fig. 2. Eddy current measurements of the quantitative readout gradient waveforms on a typical cone. (a) Measured gradient waveforms along three axes (X, solid line; Y, dotted line; Z dashed line), (b) K-space deviation due to linear eddy currents from the ideal trajectories in (a) normalized by the desired k-space sampling interval dk (=FOV^{-1}). (c) Accumulated phase due to B_0 eddy currents during the readout duration of ~9.8 ms.

3.3. Motion detection and correction

Fig. 5a shows representative navigator images of the same image partition during one 3D image acquisition where movements were introduced between the adjacent navigator acquisitions. Eight complete navigator frames were collected. Due to the long T2 of CSF and short T2 of brain tissue, the navigator signal acquired with a relatively longer echo time was dominated by the signal from CSF, which provides high spatial frequency features with high SNR that are beneficial for image registration. The derived rigid body translational and rotational motion parameters on all three axes are plotted in Fig. 5b and c, respectively. The first navigator frame was used as the reference for motion detection. Various degree of motion was detected as the subject was instructed to deliberately cough and/or adjust his head location in a random fashion at the beginning of the 2nd–7th navigator frames. Relatively large shifts of up to 5 mm and rotations of up to 7° were detected.

The motion parameters derived from the navigator acquisitions were used to correct for motion in the normal quantitative imaging data in Fig. 6, where four representative slices from the volume acquisition are shown without and with motion correction. The images are blurry due to motion in Fig. 6a, while significant improvement in image sharpness is readily visible in all slices in Fig. 6b. The signal intensity profiles in Fig. 6c of the same cross section location (horizontal lines in Fig. 6a and b) again show improvement in image sharpness after motion correction. The relative positions of the CSF features in the profiles are misaligned as a result of the motion.

3.4. Impact of motion and motion correction on TSC quantification

Fig. 7 shows the effectiveness of the navigator motion correction in reducing the errors of quantitative sodium imaging. Three TSC maps (**A**: no motion, $\mathbf{B_{unc}}$: with motion before motion correction, $\mathbf{B_{nav}}$: with motion after motion correction) are visually simi-

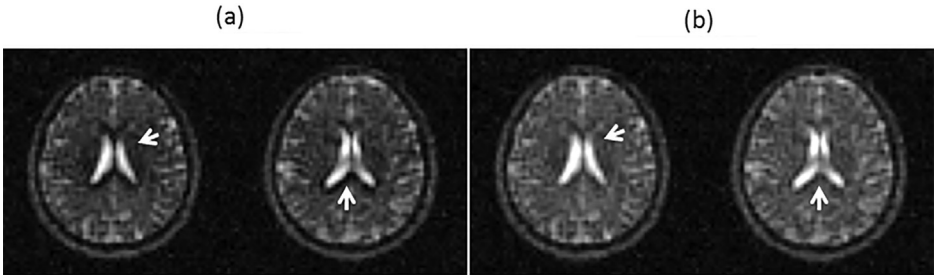

Fig. 3. Impact of eddy current correction on image. (a) Reference images (no motion) reconstructed without eddy current correction show darker center and rim around the bright ventricles (arrows). (b) Corresponding images reconstructed with eddy current correction show improved signal intensity homogeneity and minimal dark rim around the ventricles (arrows).

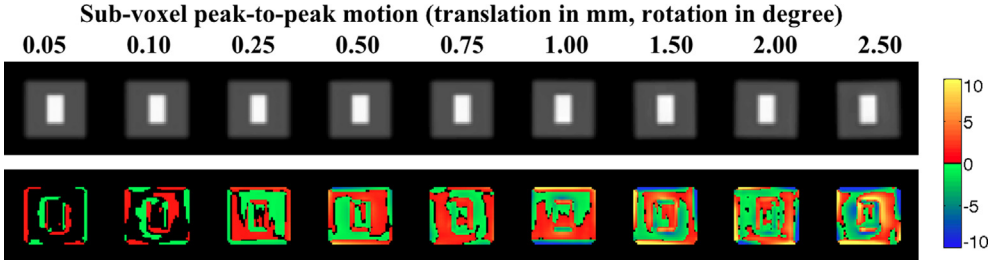

Fig. 4. Motion simulation model with simulated translations and rotations showing (top row) single quantitative image through the phantom and (bottom row) map of the TSC difference (%) between stationary and moving model in color. Color scale is percent difference in TSC. The selected models shown are given for simulations where translations (mm) and rotations (°) have the same values as given in the numbers above the images. The color-scale was chosen to facilitate the visualization of motion induced quantification errors greater than 5%.

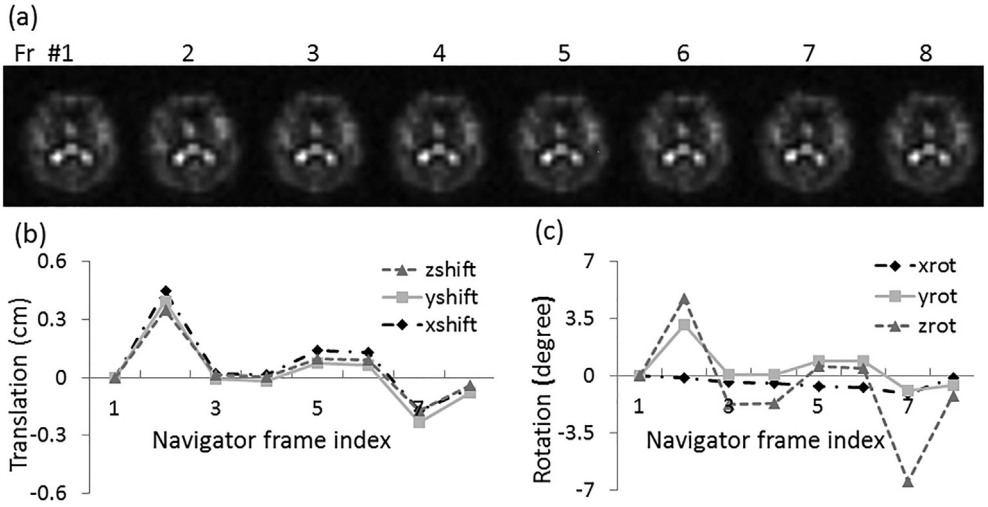

Fig. 5. (a) Eight frames of navigator images of the same partition during the acquisition of a single quantitative sodium dataset, which were used to derive (b) translational and (c) rotational motions on three axes during eight equal segments of the total acquisition.

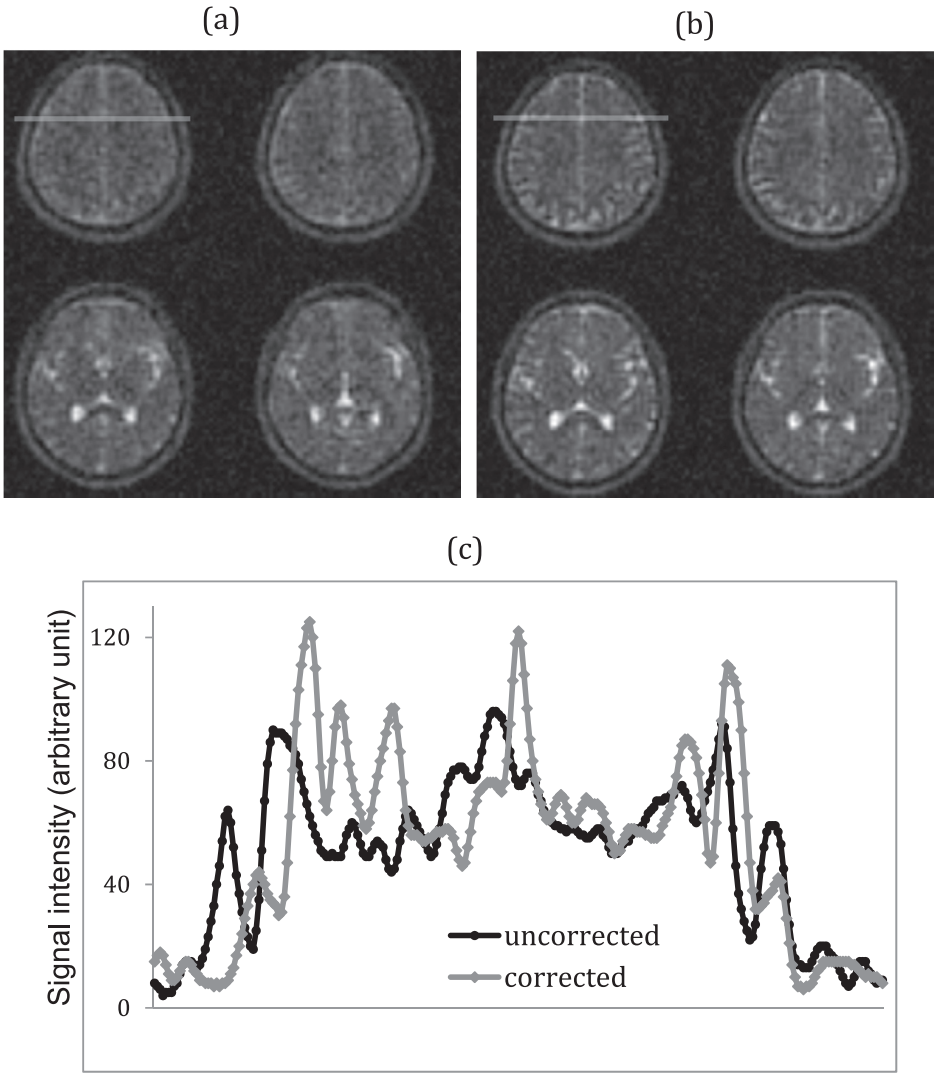

Fig. 6. Representative human brain images at four slice locations before (a) and after (b) motion correction using the eight navigator images acquired across the quantitative sodium image, and (c) profiles of the sodium signal in the same cross-section before and after motion correction as indicated by the horizontal lines in (a) and (b). Significant improvement in image sharpness can be appreciated after correction. The profiles show the sodium signal in order: air, extracranial soft tissues, skull, subarachnoid space, brain tissue, interhemispheric fissure, brain tissue, subarachnoid space, skull, extra cranial soft tissues, air. The displacement of the profiles is due to the head motion.

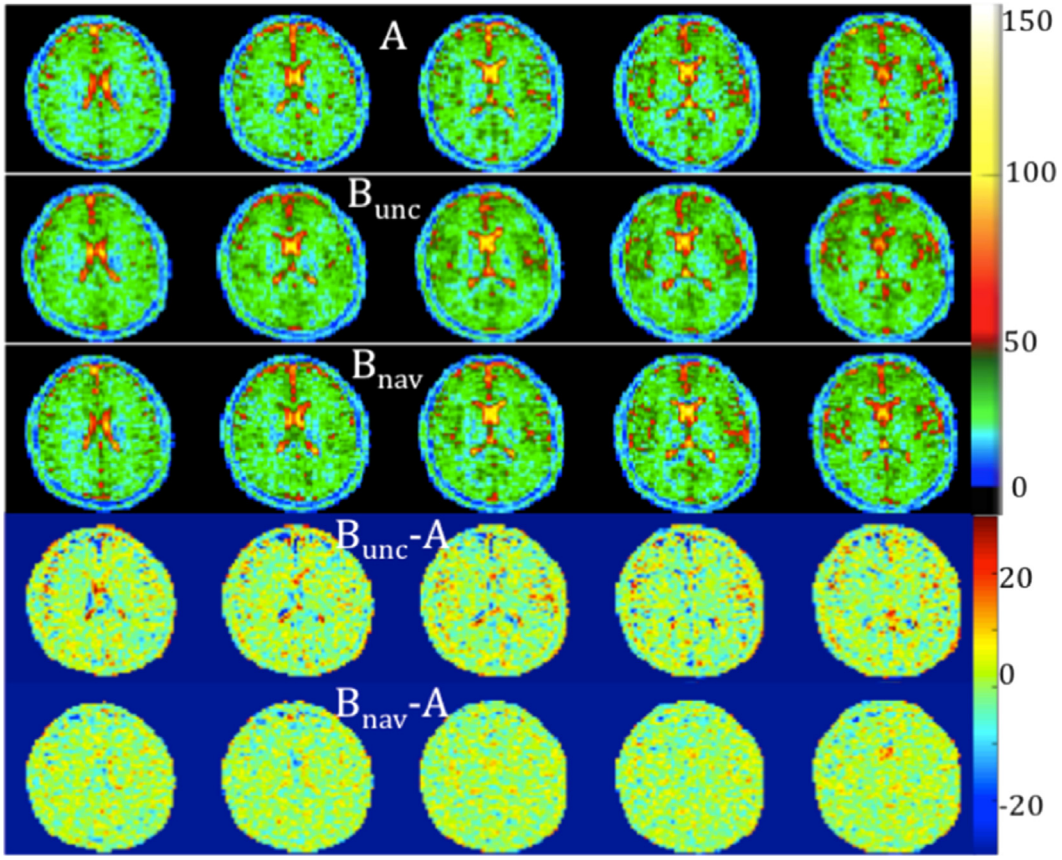

Fig. 7. Quantitative TSC maps of the human brain (**A**) without motion, ($\mathbf{B_{unc}}$) with discrete coughing without motion correction and ($\mathbf{B_{nav}}$), with discrete coughing and navigator motion correction. The quantification errors seen in the difference map without motion correction (B_{unc} –A) is greatly reduced following navigator motion correction (B_{nav} – A). The units of the color scales are in mmol/L of tissue.

lar. A non-linear color-scale scheme is used to emphasize the relatively narrow TSC range in the brain parenchyma compared to the wide biological range that includes CSF. This scale enhances detection of parenchymal variations that are often of biological interest. The difference images $\mathbf{B_{unc}}$ – **A** reveal significant quantification error (up to ±20 mmol/L of tissue) due to motion induced by coughing. After motion correction $\mathbf{B_{nav}}$ **– A**, the error in tissue is mostly reduced to below ±5 mmol/L, an error that is now similar to the standard deviation of TSC in brain parenchyma voxels determined by the SNR of sodium imaging. Again, the color-scale of the difference images was chosen to facilitate the visualization of the differences greater than 5 mmol/L before and after motion correction. The largest residual error after motion correction is primarily seen in the CSF spaces, which may be partly due to CSF flow that violates the rigid body assumption.

4. Discussion

Despite efficient acquisition strategies, quantitative sodium MR imaging requires not only a quantitative acquisition lasting ~10 min but often additional acquisitions to correct B1 and B0 inhomogeneities that compromise accuracy. Even for cooperative patients, head motion occurs during such extended periods. The simulation and experiments show that motion is yet another source of significant quantification error, even though the flexTPI acquisition trajectories are relatively resilient to motion as compared to Cartesian acquisitions. The proposed navTPI sequence segments the long quantitative acquisition time into multiple short periods in which lower resolution navigator images can be obtained without time penalty. These navigator images allow for estimation of rigid motion parameters that allow segmented motion correction of the k-space data of the quantitative acquisition. Image blurring and quantification errors in TSC maps are significantly reduced after motion correction.

Motion correction for sodium imaging using ECG-gating or self-gating has been reported for correcting the periodical cardiac motion or respiratory motion [34,35]. These methods are not directly applicable for correction of the occasional/random motion, such as cough or head position adjustment during imaging for which the proposed navigator method has been shown to be applicable. The temporal resolution of motion detection can be improved using the moving window approach – i.e., reconstructing navigator echo images within a moving window across the acquired navigator echo data. In this way, the nominal temporal resolution of the navigator frames can be made as high as one TR. However, the motion happening during any navigator frame will compromise the accuracy of motion detection and consequently decrease the effectiveness of this correction. The acquisition time of ~70 s for each navigator frame in this work can be significantly shortened by imaging at an even lower spatial resolution (e.g., to 15 mm isotropic resolution as compared to the 8 mm used here could shorten the acquisition time for each time frames to ~20 s or less), using more efficient k-space sampling trajectories such as 3D Cones [16] for navigator acquisition, or using fast imaging techniques such as parallel imaging. Despite the low spatial resolution, reasonable image registration can be achieved because the long TE used for the navigator acquisition and the differences in tissue transverse relaxation times isolates high spatial frequency features by effectively segmenting CSF spaces from brain tissues.

As the eddy currents for our 9.4 T scanner were significantly larger than those previously reported in [15] on our 3 T clinical scanner, eddy current correction was critical to improve the accuracy of TSC quantification. As a volume transmit proton coil at 9.4 T was not available when this work was performed, eddy current characterization based on proton signals was not feasible. The method used in [15,22] requires acquiring calibration data from multiple thin (~1mm) slices at different off-isocenter distances. Due to the much lower gyromagnetic ratio of sodium as compared to that of proton, extremely high gradient amplitudes would have been needed to selectively excite a thin slice with a resultant relatively long TE. Thus that approach was not used to acquire eddy current correction data with the sodium signal. Rather, the Fourier encoding method proposed in [21] was adopted and extended to directly measure the actual k-space trajectories (including linear eddy current effects) and phase due to B_0 eddy currents. The Fourier encoding method also has a SNR advantage as signal from the entire volume instead of a thin slice was acquired in each TR during the entire calibration acquisition. Other methods using models such as multiple exponentials to characterize eddy currents have been proposed to correct for eddy currents during sodium MR imaging at 9.4 T [36]. The performance of these eddy current correction methods needs further investigation.

5. Conclusion

Navigator data obtained from echoes added to the flexTPI sequence enables intra-acquisition motion correction to improve the accuracy of quantitative sodium MR imaging without time penalty. Further study is needed to improve the navigator echo image frame rate.

6. Grant support

Financial support is gratefully acknowledged from PHS grants RO1 NS386760 and RO1 CA129553.

References

[1] K.R. Thulborn, T.S. Gindin, D. Davis, P. Erb, Comprehensive MRI protocol for stroke management: tissue sodium concentration as a measure of tissue viability in a non-human primate model and clinical studies, Radiology 139 (1999) 26–34.
[2] K.R. Thulborn, D. Davis, J. Snyder, H. Yonas, A. Kassam, Sodium MR imaging of acute and subacute stroke for assessment of tissue viability, Neuroimag. Clin. N. Am. 15 (2005) 639–653.
[3] L.P. Nunes Neto, G. Madelin, T.P. Sood, C.C. Wu, D. Kondziolka, D. Placantonakis, J.G. Golfinos, A. Chi, R. Jain, Quantitative sodium imaging and gliomas: a feasibility study, Neuroradiology 60 (8) (2018) 795–802.
[4] K.R. Thulborn, A. Lu, I.C. Atkinson, M. Pauliah, K. Beal, T.A. Chan, A. Omuro, J. Yamada, M.S. Bradbury, Residual tumor volume, cell volume fraction and tumor cell kill during fractionated chemoradiation therapy of human glioblastoma using quantitative sodium MR imaging, Clin. Cancer Res. (2018), https://doi.org/10.1158/1078-0432.CCR-18-2079, Pii clincanres.2079.
[5] K.R. Thulborn, Quantitative sodium MR imaging: a review of its evolving role in medicine, Neuroimage 168 (2018) 250–268.
[6] E.A. Mellon, D.T. Pilkinton, C.M. Clark, et al., Sodium MR imaging detection of mild Alzheimer disease: preliminary study, AJNR Am. J. Neuroradiol. 30 (5) (2009) 978–984.
[7] K.R. Thulborn, Quantitative sodium MR Imaging: a review of its evolving contribution to medicine, Neuroimage 2016 (168) (2016) 250–268.
[8] A.M. Grapperon, B. Ridley, A. Verschueren, A. Maarouf, S. Confort-Gouny, E. Fortanier, L. Schad, M. Guye, J.P. Ranjeva, S. Attarian, W. Zaaraoui, Quantitative brain sodium MRI depicts corticospinal impairment in amyotrophic lateral sclerosis, Radiology 292 (2019) 422–428.
[9] D. Burstein, C.S. Springer Jr., Sodium MRI revisited, Magn. Reson. Med. 82 (2019) 521–524.
[10] K. Huhn, T. Engelhorn, R.A. Linker, A.M. Nagel, Potential of sodium MRI as a biomarker for neurodegeneration and neuroinflammation in multiple sclerosis, Front. Neurol. 10 (84) (2019).
[11] M. Petracca, L. Fleysher, N. Oesingmann, M. Inglese, Sodium MRI of multiple sclerosis, NMR Biomed. 29 (2) (2016) 153–161.
[12] G.G. Somjen, Ions of the Brain, Normal Function, Seizures and Stroke, Oxford University Press. New York, New York, 2004.
[13] F.E. Boada, J.S. Christensen, J.S. Gillen, K.R. Thulborn, Three dimensional projection imaging with half the number of projections, Magn. Reson. Med. 37 (1997) 470–477.
[14] A.M. Nagel, F.B. Laun, M.A. Weber, C. Matthies, W. Semmler, L.R. Schad, Sodium MRI using a density-adapted 3D radial acquisition technique, Magn. Reson. Med. 62 (2009) 1565–1573.
[15] A. Lu, I.C. Atkinson, T. Claiborne, F. Damen, K.R. Thulborn, Quantitative sodium imaging with a flexible twisted projection pulse sequence, Magn. Reson. Med. 63 (2010) 1583–1593.
[16] P.T. Gurney, B.A. Hargreaves, D.G. Nishimura, Design and analysis of a practical 3D cones trajectory, Magn. Reson. Med. 55 (2006) 575–582.
[17] R.L. Ehman, J.P. Felmlee, Adaptive technique for high-definition MR imaging of moving structures, Radiology 173 (1989) 255–263.
[18] A.J.W. van der Kouwe, T. Benner, A.M. Dale, Real-time rigid body motion correction and shimming using cloverleaf navigators, Magn. Reson. Med. 56 (2006) 1019–1032.
[19] L. Qin, P. van Gelderen, J.A. Derbyshire, F. Jin, J. Lee, J.A. de Zwart, Y. Tao, J.H. Duyn, Prospective head movement correction for high resolution MRI using an in-bore optical tracking system, Magn. Reson. Med. 62 (4) (2009) 924–934.
[20] F. Godenschweger, U. Kagebein, D. Stucht, U. Yarach, A. Sciarra, R. Yakupov, F. Lusebrink, P. Schulze, O. Speck, Motion correction in MRI of the brain, Phys. Med. Biol. 61 (5) (2016) R32–R56, https://doi.org/10.1088/0031-9155/61/5/R32.
[21] M.T. Alley, G.H. Glover, N.J. Pelc, Gradient characterization using a Fourier-transform technique, Magn. Reson. Med. 39 (1998) 581–587.
[22] A. Lu, B.L. Daniel, J.M. Pauly, Pauly K. Butts, Improved slice selection with eddy current compensation for R2* mapping during cryoablation, J. Magn. Reson. Imag. 28 (2008) 190–198.
[23] S.B. Reeder, A.Z. Faranesh, E. Atalar, E.R. McVeigh, A novel object-independent "balanced" reference scan for echo-planar imaging, JMRI. 9 (1999) 847–852.
[24] A. Lu, I.C. Atkinson, J.T. Vaughn, K.R. Thulborn, Impact of gradient timing error on the tissue sodium concentration bioscale measured using flexible twisted projection imaging, J. Magn. Reson. 213 (2011) 176–181.
[25] K.R. Thulborn, The challenges of integrating a 9.4T MR scanner for human brain imaging, in: P.-M. Robitaille, L.J. Berliner (Eds.), Ultra High Field Magnetic Resonance Imaging, Springer Science and Business Media, 2006, pp. 105–126..
[26] I.C. Atkinson, L. Renteria, H. Burd, N.H. Pliskin, K.R. Thulborn, Safety of Human MRI at Static Fields Above the FDA 8T Guideline: Sodium Imaging at 9.4T Does Not Affect Vital Signs or Cognitive Ability, J. Magn. Reson. Imag. 26 (2007) 1227–1252.
[27] I.C. Atkinson, R. Sonstegaard, N.H. Pliskin, K.R. Thulborn, Vital signs and cognitive function are not affected by 23-sodium and 17-oxygen MR imaging of the human brain at 9.4 Tesla, J. Magn. Reson. Imag. 32 (2010) 82–87.
[28] A. Heinrich, A. Szostek, P. Meyer, F. Nees, J. Rauschenberg, J. Gröbner, M. Gilles, G. Paslakis, M. Deuschle, W. Semmler, H. Flor, Cognition and sensation in very high static magnetic fields: a randomized case-crossover study with different field strengths, Radiology 266 (2013) 236–245.
[29] J. Rauschenberg, A.M. Nagel, S.C. Ladd, J.M. Theysohn, M.E. Ladd, H.E. Möller, R. Trampel, R. Turner, R. Pohmann, K. Scheffler, A. Brechmann, J. Stadler, J. Felder, N.J. Shah, W. Semmler, Multicenter study of subjective acceptance during magnetic resonance imaging at 7 and 9.4 T, Invest. Radiol. 49 (2014) 249–259.
[30] R.P. Woods, S.T. Grafton, C.J. Holmes, S.R. Cherry, J.C. Mazziotta, Automated image registration: I. General methods and intrasubject, intramodality validation, J. Comput. Assist. Tomogr. 22 (1998) 139–152.
[31] R.P. Woods, S.T. Grafton, J.D.G. Watson, N.L. Sicotte, J.C. Mazziotta, Automated image registration: II. Intersubject validation of linear and nonlinear models, J. Comput. Assist. Tomogr. 22 (1998) 153–165.
[32] I.C. Atkinson, A. Lu, K.R. Thulborn, Preserving the accuracy and resolution of the sodium bioscale from quantitative sodium MRI during intra-subject alignment across longitudinal studies, Magn. Reson. Med. 68 (3) (2012) 751–1661.
[33] L.C. Man, J.M. Pauly, A. Macovski, Multifrequency interpolation for fast off-resonance correction, Magn. Reson. Med. 37 (1997) 785–792.
[34] T. Platt, R. Umathum, T.M. Fiedler, A.M. Nagel, A.K. Bitz, F. Maier, P. Bachert, M. E. Ladd, M.O. Wielpütz, H.U. Kauczor, N.G.R. Behl, In vivo self-gated $_{23}$ Na MRI at 7 T using an oval-shaped body resonator, Magn. Reson. Med. 80 (2018) 1005–1019.
[35] R. Jerecic, M. Bock, S. Nielles-Vallespin, C. Wacker, W. Bauer, L.R. Schad, ECG-gated 23Na-MRI of the human heart using a 3D-radial projection technique with ultra-short echo times, Magn. Reson. Mater. Phy. 16 (2004) 297–302.
[36] I.C. Atkinson, A. Lu, K.R. Thulborn, Characterization and correction of system delays and eddy currents for MR imaging with ultrashort echo-time and time-varying gradients, Magn. Reson. Med. 62 (2) (2009) 532–537.